Journal of Applied Fluid Mechanics, Vol. 16, No. 11, pp. 2206-2218, 2023.
Available online at www.jafmonline.net, ISSN 1735-3572, EISSN 1735-3645.
https://doi.org/10.47176/jafm.16.11.1857

Three-Dimensional Optimization of Blade Lean and Sweep for an Axial Compressor to Improve the Engine Performance

M. Heidarian Shahri, A. Madadi† and M. Boroomand

Amirkabir University of Technology, Tehran, Iran

†*Corresponding Author Email: ali.madadi@aut.ac.ir*

ABSTRACT

Nowadays, optimization methods have been considered as a practical tool to improve the performance of turbo-machines. For this purpose, the numerical study of the aerodynamic flow of the NASA Rotor-67 axial compressor has been investigated, and the results of this three-dimensional simulation show good agreement with experimental data. Then, the blade stacking line is changed using lean and sweep for Rotor-67 to improve the compressor performance. The third-order polynomial is selected to generate the lean and sweep changes from the hub to the shroud. The compressor flow field is solved by a Reynolds averaged Navier-Stokes solver. The genetic algorithm, coupled with the artificial neural networks, is implemented to find the optimum values for blade lean and sweep. Considering the three objective functions of pressure ratio, mass flow rate, and isentropic efficiency, the optimized rotor is obtained using the optimization algorithm. Two geometries are obtained using the optimization algorithm. The results of the optimized compressor include improving the isentropic efficiency, pressure ratio, and mass flow equal to 0.57%, 0.93%, and 1.8%, respectively. After compressor optimization, the effect of the changes in the compressor performance parameters is studied on a single spool turbojet engine. The engine is modeled by analyzing the Brayton thermodynamic cycle of the assumed turbojet engine under design point operating conditions. Results show that for the best test case, the engine with the optimized rotor, the thrust, and SFC are improved by 1.86% and 0.21%, respectively.

Article History

Received March 10, 2023
Revised May 7, 2023
Accepted June 21, 2023
Available online September 3, 2023

Keywords:

Compressor
Optimization
Lean
Sweep
Gas Turbine

1. INTRODUCTION

The axial compressor is one of the most important components of gas turbine engines. The performance enhancement of the compressors can directly improve engine performance. Recently, computational fluid dynamics (CFD) has been one of the essential tools used by researchers to improve the performance of turbo-machineries. To achieve this purpose, optimization methods are utilized coupled with computational fluid dynamics to solve the flow field of the turbo-machines. Reducing the number of costly and time-consuming experiments and obtaining details of flow behavior in the turbo-machines are the most important benefits of the optimization methods. Some objectives of optimization methods in turbo-machinery problems are reducing weight, increasing total pressure ratio, and isentropic efficiency.

Several researchers have developed methods to improve the performance of axial compressors (Hah & Wennerstrom, 1990; Jang, et al. 2005; Benini & Biollo, 2006; Razavi & Boroomand, 2014; Wang et al. 2021; Yu, et al. 2022; Lu et al. 2023). Furthermore, the effects of sweep on the axial compressor (NASA Rotor-37) which had a grooved casing were numerically simulated by Goswami & Govardhan (2019) with the aim of improving the stall margin.

The effects of lean and sweep blades on the performance of NASA Rotor-37 and Rotor-67 have been studied by Denton & Xu (2002). These aerodynamic effects have been investigated to improve the performance of the fan shock wave profile. Increasing the stall margin and increasing the operating range at maximum efficiency for downstream sweep profiles are the results of this study.

NOMENCLATURE

a, b, c, d	Coefficients of a third-order polynomial	D	Design
ANN	Artificial Neural Network	in	Inlet
k	The ratio of specific heats	is	Isentropic
$\dot{m}$	Mass flow rate [kg/s]	out	Outlet
Obj	Objective function	η	Isentropic Efficiency
PR	Pressure ratio	δ	Displacement
s	Span normalized		

Benini performed a three-dimensional multi-objective optimization on the NASA Rotor-37, a transonic rotor, with the aim of achieving maximum isentropic efficiency and maximum pressure ratio under the constraint of mass flow rate (Benini, 2004). The results showed that the optimal geometry provided a 1.5% improvement in isentropic efficiency and indicated the optimal sweep angle for rotor rotation.

Oyama et al developed a high-precision code for optimal design and optimization of turbomachinery to enhance the performance of NASA Transonic Rotor 67 (Oyama et al. 2004). The results showed a significant improvement in the pressure ratio, isentropic efficiency, and choked mass flow rate, by 0.6%, 1.78%, and 0.46%, respectively.

A three-dimensional optimization based on the change of the stacking line using computational fluid dynamics simulation was performed by Samad and Kim (2008), resulting in an improvement of 0.51% for efficiency and 1.25% for pressure ratio.

Wang used the coupled of Multi-objective genetic algorithms and approximation models to improve the performance of NASA Rotor-37 (Wang et al. 2011) and the results include 1.0% enhancement in pressure ratio, 1.1% efficiency and -0.04% for choked mass flow rate.

Another study was conducted on the optimization of the effects of lean and sweep on the performance improvement of NASA Rotor-37 by Huang et al. (2019). Computational fluid dynamics simulation was used to simulate the aerodynamic field of the blade which stacking line has changed using C and S curves and resulting in an increase in the isentropic efficiency at the design point with a mass flow rate constraint. The peak efficiency was increased 1.1%, peak total pressure ratio increased 1.6% and the absolute value of stall margin increased 2% compared to Rotor-37.

Optimization research has been performed on a single-stage axial compressor with lean and sweep blade effects by Wang et al to improve the isentropic efficiency and stall margin (Wang et al. 2020). In this research, a three-dimensional numerical simulation of the compressor is performed, and then the genetic algorithm and neural network coupling are performed to improve the compressor performance at three design points, close to the stall and chock regime.

A study was conducted to investigate the effects of using lean on controlling flow separation on the blade surface and improving the performance of turbomachinery by Cao et al. (2021). So, the positive and negative effects of lean on a transonic rotor were numerically analyzed. The results showed that the optimization of lean could lead to maximum isentropic efficiency and a suitable range of flexibility for performance improvement.

A study conducted by Wang et al investigated the effects of using lean sweep and end bend to improve the aerodynamic performance of NASA's transonic Rotor-37 (Wang et al. 2022). In an optimization process using coupled numerical analysis with Shapley Additive Explanations (SHAP), the sensitivity effects of design variables on geometry were evaluated. The results of the study showed that the tip sweep had the greatest impact on isentropic efficiency.

As mentioned, three-dimensional optimization of the compressor with the aim of lean and sweep has been proposed by many researchers. In this paper, the Genetic algorithm coupled with an Artificial Neural Network is used to optimize NASA Rotor-67. The three-dimensional performance of the compressor is investigated using a three-dimensional Reynolds-average Navier-Stokes flow solver.

Using a third order polynomial equation with coefficients in a curve provides greater flexibility in modifying the stacking-line, leading to optimal 3D blade designs. This method is applied simultaneously to both the lean and sweep of the blade. Although it may increase the number of design variables and complexity of the problem, successful solutions have been achieved for 3D optimization. Additionally, incorporating geometric constraints at the root of the blade to eliminate stress concentration has led to valid solutions for optimal 3D aerodynamic geometries.

Then, the results of this optimization compared to other studies, the thermodynamic cycle analysis has been evaluated after numerical simulation. So, the effect of compressor optimization is studied on a single spool turbojet engine at on-design condition. To do so, Rotor-67 is considered as the first stage of the axial compressor of the engine, and the engine thrust and SFC are investigated, respectively.

2. CFD SIMULATION OF NASA ROTOR-67

In this paper, NASA rotor-67, an axial-flow rotor, is used as the test case for blade shape optimization. It is the first stage rotor of a two-stage fan and is designed as a low-aspect-ratio transonic rotor with 22 blades. The meridional and three-dimensional views of the measurement stations are shown in Fig. 1. Stations 1 and 2 (upstream and downstream of the rotor, respectively)

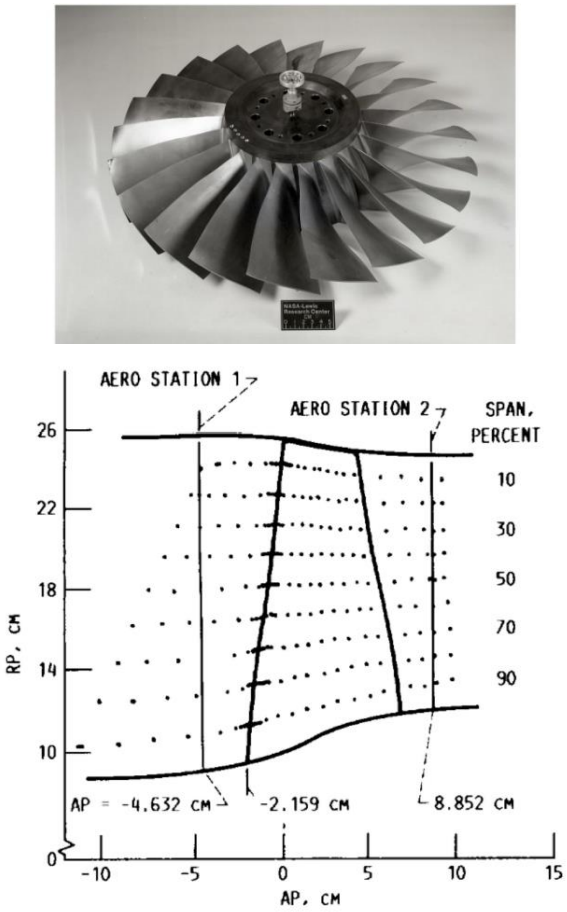

Fig. 1 NASA Rotor-67 at three-dimensional (Top) and meridional views (Bottom) (Strazisar et al. 1989)

Table 1 NASA Rotor-67 design point specifications.

Pressure Ratio	1.632
Efficiency	0.919
Mass Flow Rate [kg/s]	33.794
Rotational Speed [rpm]	16043
Inlet hub-tip ratio	0.375
Inlet tip relative Mach number	1.38
Tip solidity	1.29
Rotor aspect ratio	1.56
Number of blades	22

are used to measure the overall performance of the rotor (Strazisar et al.1989).

The rotor design pressure ratio is 1.63 at the atmospheric condition (1 [atm] and 288.15 [K]). The design rotational speed is 16 043 [rpm], which yields a tip speed of 429 [m/sec] and a relative Mach number of 1.38 at the inlet tip. The aspect ratio of the rotor based on average span/root axial chord is 1.56. The solidity of rotor varies from 3.11 at the hub to 1.29 at the tip. The inlet and exit tip diameters are 51.4 and 48.5 [cm], and the inlet and exit hub/tip radius ratios are 0.375 and 0.478, respectively. The tip clearance is approximately 1.0 [mm] (Strazisar et al. 1989). The detailed specifications of the axial compressor are

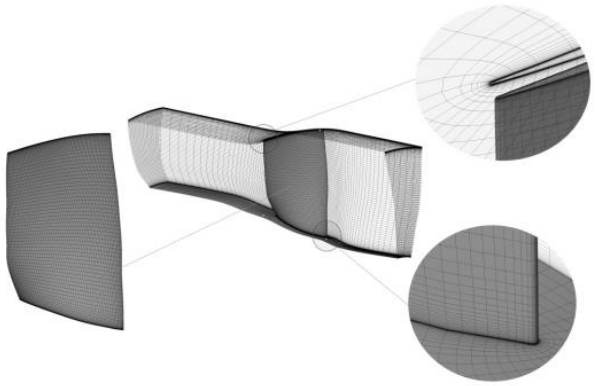

Fig. 2 The medium structured Grids for NASA Rotor-67

summarized in Table 1. More details about the Rotor-67 flow field data can be found at (Strazisar et al. 1989).

The values presented in the table are used as the operating conditions in this research and as the reference values for comparing the optimum performance.

A three-dimensional finite volume solver has been used to simulate the aerodynamic flow field of axial compressor. The equations are solved using a pressure-based method. The viscous effects are considered using Reynolds-average Navier-Stokes code (RANS) based on the SST turbulence model.

A composite grid system with structured H-, C-, and O-type grids is adopted to represent the complicated configuration of the axial compressor. Figure 2 shows the computational blocks and grids.

A three-dimensional Reynolds-average Navier-Stokes code (RANS) based on the SST turbulence model (Menter et al. 2003) is used to solve the compressor flow field. To reduce the computational cost, one blade grid is generated and used in the solution with the boundary conditions of periodic surfaces. The boundary conditions are presented in Fig. 3.

Inlet air with atmospheric conditions (total pressure 1 [atm] and total temperature 288.15 [K]) enters normal to inlet boundary. The aerodynamic field of the Rotor-67 is rotating at a rotational speed, while the Inlet and Outlet domains are considered stationary domains. The value of outlet static pressure also depends on the operating conditions.

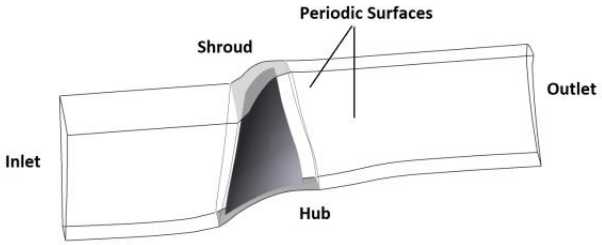

Fig. 3 Computational domain and boundary conditions for NASA Rotor-67

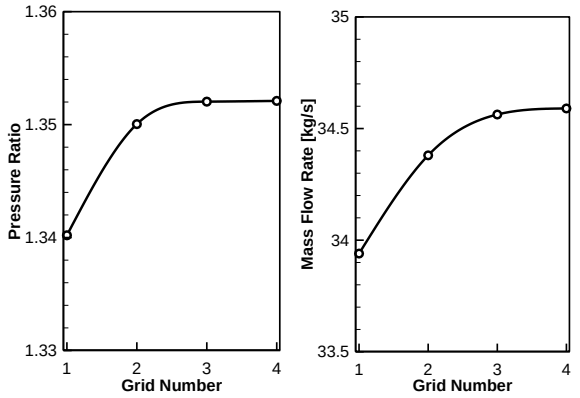

Fig. 4 Grid study of CFD results for NASA Rotor-67

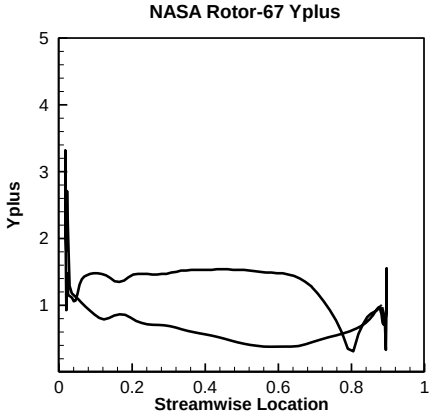

Fig. 5 NASA Rotor-67 Yplus distribution of Grid no. 3

Now, to study the independence of the results from the number of elements, four grids with 480,000, 720,000, 1,360,000, and 1,780,000 elements are generated. The results of performance parameters are compared in Fig. 4 for these four grids.

According to the results of the grid study, it can be concluded that grid number three can be chosen to simulate the NASA Rotor-67 flow field within the optimization procedure. To check the validity of the Yplus number, the distribution of Yplus near the blade surfaces of grid number three is plotted in Figure 5. It is clear that the Yplus average of the blade surfaces for grid no.3 is less than 5 (about 2.5), which is within the turbulence model's valid range.

3. CFD SOLVER VALIDATION

To validate the numerical results, the numerical method results are compared with the experimental data (Strazisar et al. 1989). Numerical and experimental results, including performance maps of pressure ratio and isentropic efficiency in normalized mass flow rate, are compared in Fig. 6.

The minimum and maximum pressure ratios of Rotor-67 in the numerical method have been obtained at the chocked and near the stall points, and their values are 1.28 and 1.67. The mass flow of these points is equal to

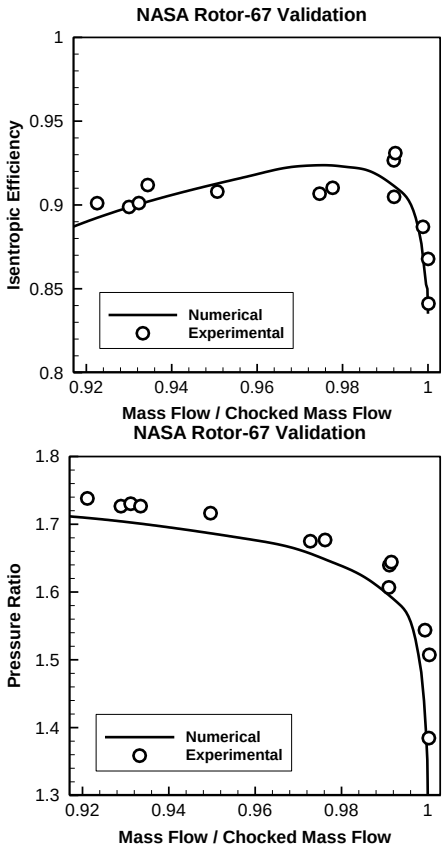

Fig. 6 Comparison of numerical results and experimental data for NASA Rotor-67

Table 2 Comparison of numerical results with experimental data at the design point

	Performance Parameters		
	Pressure Ratio	**Isentropic Efficiency**	**Mass Flow Rate [kg/s]**
Numerical	1.635	0.923	33.91
Experimental	1.632	0.919	33.79
Difference[%]	0.18 %	0.39 %	0.34 %

34.55 [kg/s] and 33.14 [kg/s], respectively. Similarly, isentropic efficiencies at chocked points and near the compressor stall have been observed to be 84% and 88%, respectively. The maximum isentropic efficiency is at the compressor design point and is equal to 92.26%; its pressure ratio is 1.635, and the mass flow rate is 33.91 [kg/s].

Additionally, the published experimental results for the values of pressure ratio, isentropic efficiency, and mass flow rate of NASA Rotor-67 at the design point have been reported as 1.632, 91.9%, and 33.794 [kg/s], respectively. The difference between the experimental data and numerical results is calculated and presented in Table 2.

According to the results of Table 2, the percentage difference of all three objective functions at the design point for the numerical method compared to the experimental data is less than 0.4 percent. Also, the relative Mach number contours of numerical result in the

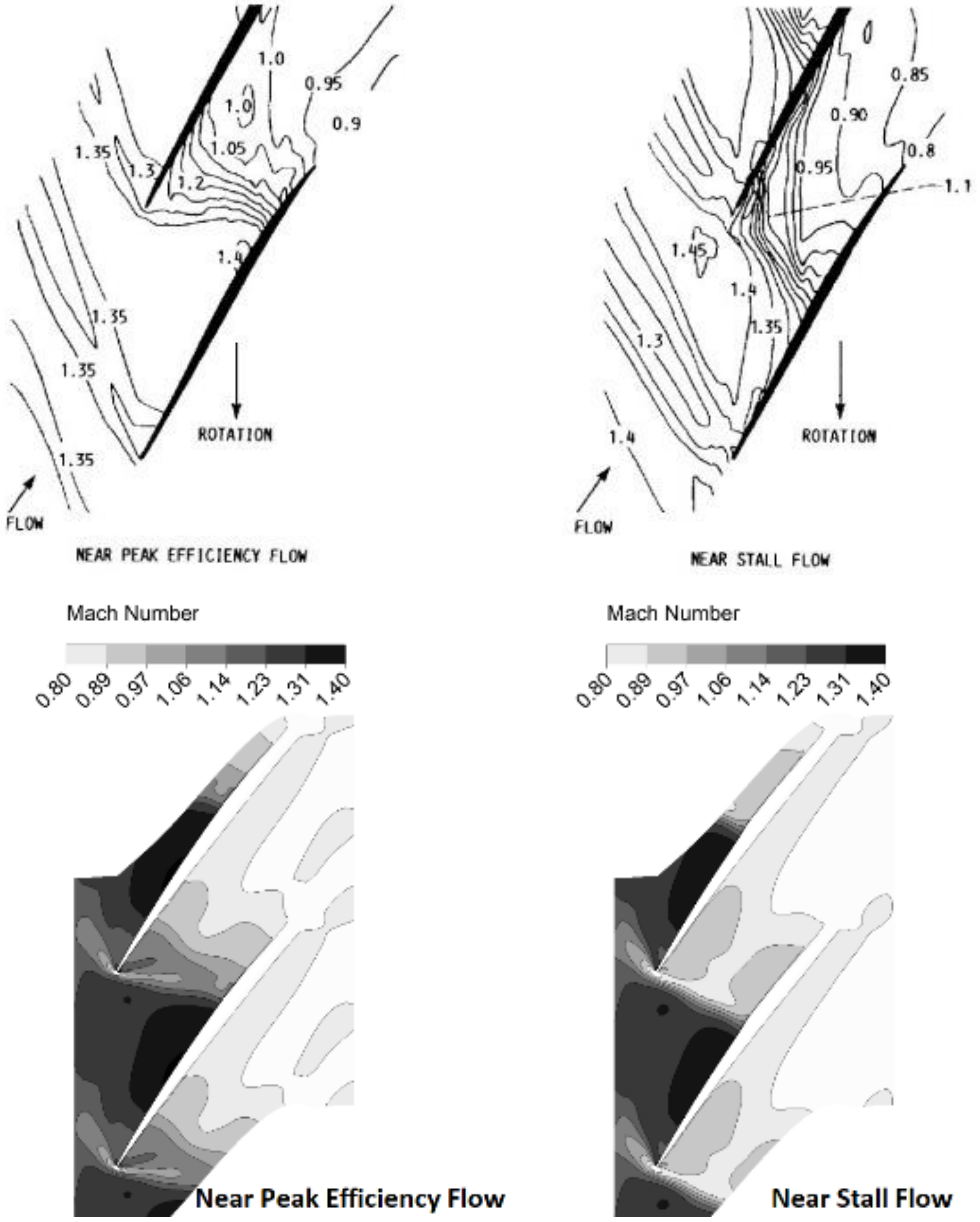

Fig. 7 Relative Mach number contours at near peak efficiency flow and near stall flow

section of 70% span are compared with the experimental ones in Fig. 7.

This relative flow Mach number trend is extracted for two points: Near peak efficiency flow and near stall flow. According to the results, the good matching of the relative Mach number behavior of the flow between the blade rows can be seen in the experimental data comparison with CFD results.

4. DESIGN PARAMETERS

This research aims to improve the compressor's performance using lean and sweep. Blade sweep is defined as the displacement of the airfoil in the axial direction (Fig. 8), and the movement towards the leading edge is considered a positive sweep. Lean is the movement of airfoil sections in the circumferential direction (Fig. 9), and the movement towards the pressure side is taken as positive lean.

Two-third order polynomials are considered for lean and sweep displacements (δ) as a function of span:

$$\delta = a \times s^3 + b \times s^2 + c \times s + d \quad (1)$$

At the hub section, the airfoil is fixed, so d must be zero. Also, to remove high-stress concentration at the root of the blade, the stacking line should be normal to the hub. It means that the first derivative of the stacking line function should be zero at the hub section. Therefore, the c coefficient is also zero. Lower and upper bounds for *a* and *b* are specified in Table 3.

Table 3 Lower and Upper bounds for lean and sweep coefficients

	Lean		**Sweep**	
Coefficients	a	b	a	b
Lower bound	-1.4	-1.4	-2.2	-2.2
Upper bound	+1.4	+1.4	+2.2	+2.2

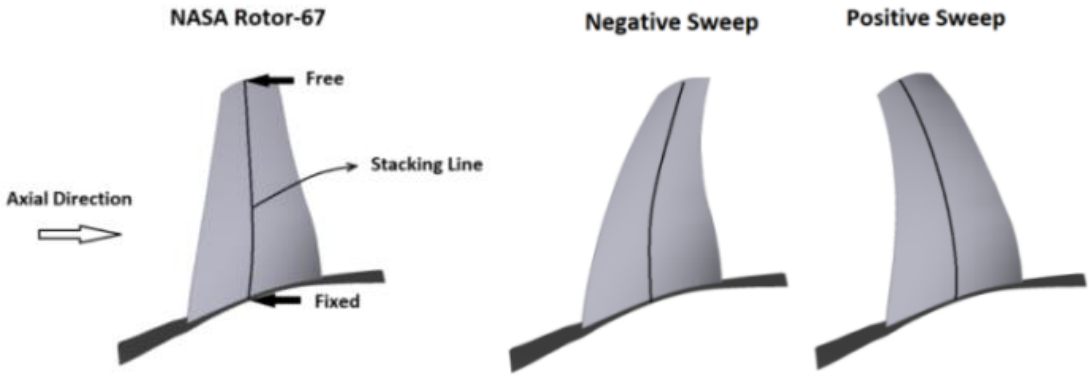

Fig. 8 Comparison of Rotor-67 with the swept blades

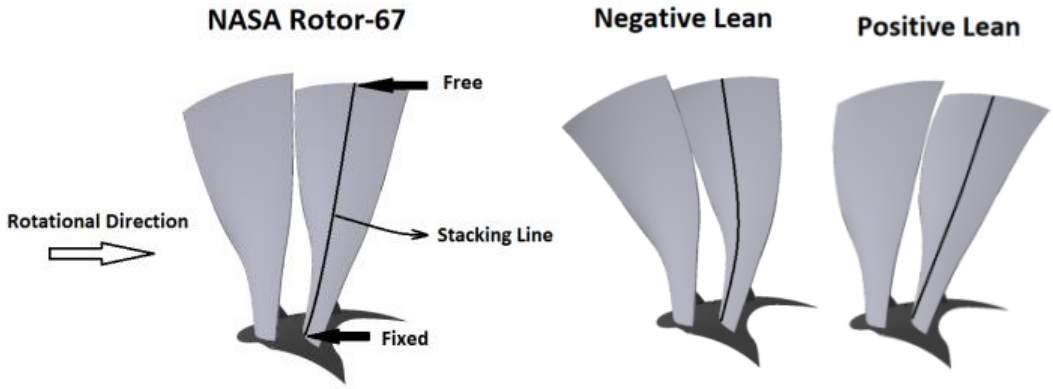

Fig. 9 Comparison of Rotor-67 with the leaned blades

Therefore, the upper and lower limits presented in Table 3 for the coefficients of the equation specify the range of the stack line and the three-dimensional blade of the compressor in the optimization.

5. OBJECTIVE FUNCTIONS

The compressor mass flow rate (m), the isentropic efficiency (η) (Eqn. (2)), and the total pressure ratio (PR) ((Eqn. (3)) are selected as the objective functions for the optimization of the rotor blade.

$$\eta = \frac{(P_{0\,out}/P_{0\,in})^{(k-1)/k} - 1}{T_{0\,out}/T_{0\,in} - 1} \tag{2}$$

$$PR = P_{0\,out}/P_{0\,in} \tag{3}$$

Where k is the ratio of specific heats, P_0 and T_0 are total pressure and total temperature, respectively.

6. OPTIMIZATION METHODOLOGY

Optimization algorithms coupled with numerical solvers have been developed to optimize geometries by researchers such as Ekradi et al. for the impeller of centrifugal compressor (Ekradi & Madadi, 2020), Ma et al. for the ring cavity in a centrifugal compressor (Ma et al. 2017) and Benini (Benini, 2004) in and axial compressor.

In this research, the genetic algorithm coupled with the artificial neural network (ANN) is implemented to find the optimum values for lean and sweep coefficients of NASA Rotor-67. At first, a random database of feasible geometries is generated. The flow field is solved using the RANS code for each geometry, and the compressor performance is obtained.

Using the generated database, three artificial neural networks are trained for three objectives: compressor isentropic efficiency, mass flow rate, and pressure ratio. Figure 10 shows the comparison of the CFD results of the database at design point as well as the results of the trained neural network with database (80 member).

Now, the Genetic algorithm is used to find the optimum of the objective function. Artificial neural networks are used to predict the objective functions instead of CFD simulations during the optimization process to reduce the computational cost.

For the optimum geometry, the flow field is solved by the RANS code to validate the results of ANNs. If the difference between the results predicted by the ANNs and the CFD solution is less than a specified tolerance, the optimization procedure is completed. Otherwise, the CFD results are added to the database, and the ANNs are trained using the updated database. The procedure is continued until the convergence criterion is met. By growing the database, the accuracy of the ANNs is improved, especially around the optimum point. The flowchart of the optimization procedure is presented in Fig. 11, and details of genetic algorithm settings are given in Table 4.

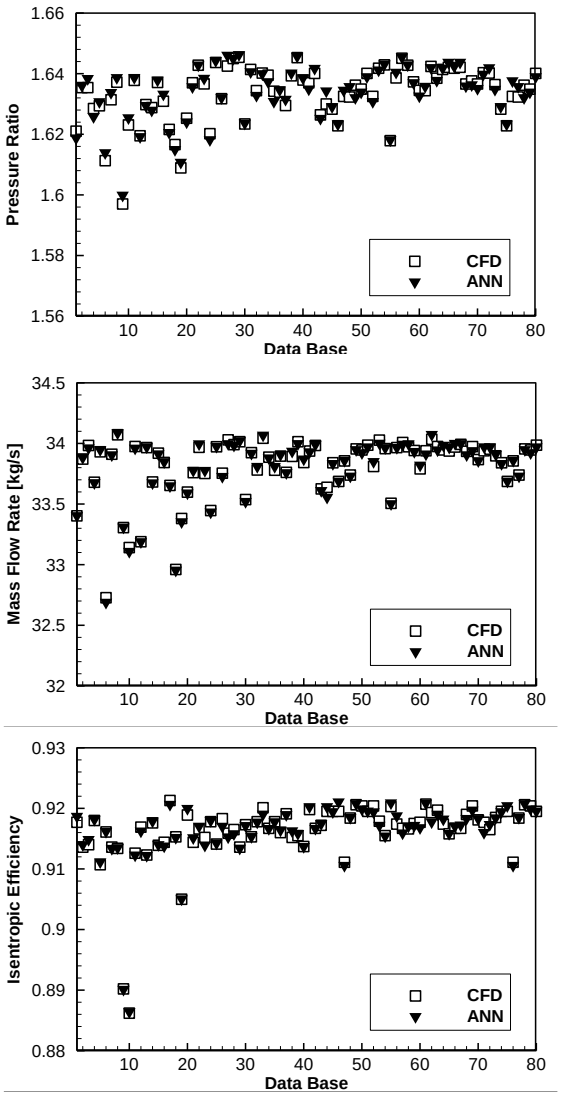

Fig. 10 Comparison of the CFD results and Artificial Neural Networks

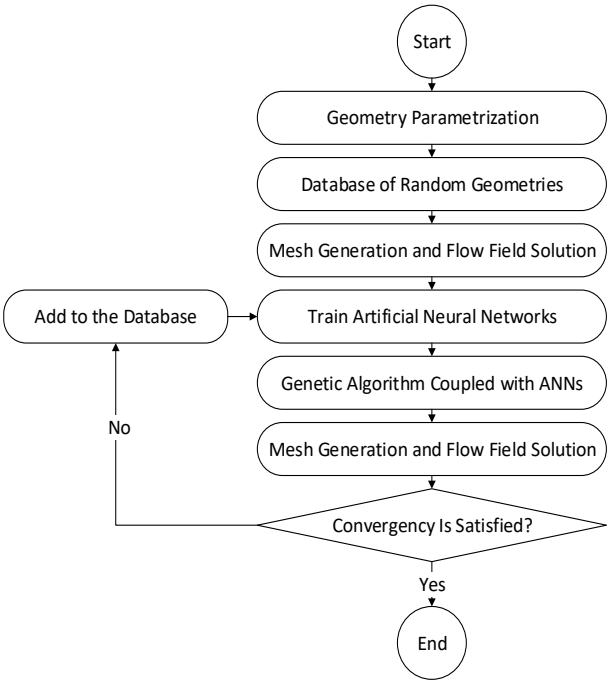

Fig. 11 Optimization procedure flowchart

Table 4 Details of the Genetic Algorithm

Criteria	Function / Value
Population Size	100
Number of Generations	100
Convergence Criteria	1e-6
Mutation	Uniform (0.1)
Selection	Uniform
Crossover	Two-point Crossover
Fitness Scaling	Rank

The genetic algorithm finds the minimum of the objective function. So, to increase the compressor isentropic efficiency, mass flow rate, and pressure ratio. The objective function is defined as:

$$\text{Obj} = (-\text{PR}) + (-\eta) + \left(-\frac{\dot{m}}{\dot{m}_D}\right) \tag{4}$$

However, in some geometry, the mass flow rate, and the pressure ratio increase while the isentropic efficiency may decrease. To overcome this challenge, both the mass flow rate and the pressure ratio are selected as the objective function, and the isentropic efficiency as the penalty function is defined to ensure that the performance of the designed compressor is not lower than the original NASA Rotor-67. The penalty function Eqn. (5) and objective function Eqn. (6) are defined.

$$\text{penalty} = \max\left(0, (\eta_D - \eta)\right) \tag{5}$$

$$\text{Obj} = (-\text{PR}) + \left(-\frac{\dot{m}}{\dot{m}_D}\right) + (10^3 \times \text{penalty}) \tag{6}$$

Also, a high weight coefficient is used in the penalty function (Eqn. (6)). Using this, the optimization algorithm will find cases where the penalty function has a more significant effect on the objective function. So, the three-dimensional optimizations of the axial compressor have been done with and without the mentioned penalty in the objective function, and the results are compared with a Rotor-67.

7. RESULTS AND DISCUSSION

At first, the results of the compressor optimization procedure are presented. These results include a performance map for design speed and distribution of compressor performance parameters from the hub to the shroud at its design point. In the second part, the effects of the optimized compressors on the engine performance are studied by modeling the thermodynamic cycle of the assumed turbojet engine at the design condition. The results include specific fuel consumption and thrust of the engine with Rotor-67 and optimized rotors.

7.1 Results of Compressor Optimization

At the first optimization step, no penalty function is considered in the objective function (Eqn. (5)). Using this objective function without penalty, one of the performance parameters of the compressor (isentropic efficiency, mass flow rate, or pressure ratio) is increased, while the other two performance parameters may be

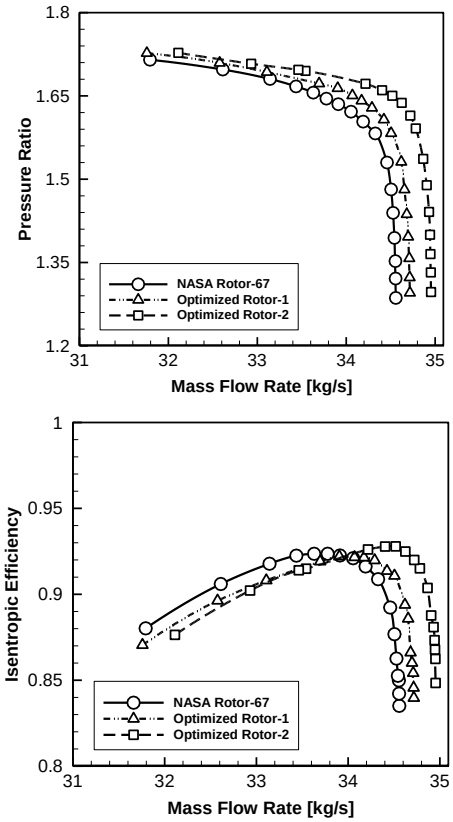

Fig. 12 Comparison of the optimized rotors and NASA Rotor-67

decreased. The penalty function is added to the objective function (Eqn. (6)) to overcome this challenge. There is no reduction in the performance parameters by applying the penalty, which is concluded by comparing the characteristic diagrams of two optimal geometries: Optimized Rotor-1 without penalty and Optimized Rotor-2 with a penalty. These optimized rotors are obtained from the optimization process and are simulated at the design speed. The performance curve for these optimized rotors is obtained by changing the outlet static pressure boundary condition. These curves are compared with the performance curve of Rotor-67 and are demonstrated in Fig. 12.

As can be seen, the performance diagrams of the optimal rotors have improved the objective functions. To evaluate the improvement percentage of performance values, the results of optimized rotors and the NASA Rotor-67 are compared at the design point in Table 5.

According to the table results, the pressure ratio is enhanced 0.38%, and mass flow of Optimized Rotor-1 is increased 0.77%, too, while the isentropic efficiency is decreased about 0.13% (There are small geometric changes with acceptable performance improvements in the Optimized Rotor-1.) Considering the penalty function, all performance parameters are improved for the Optimized Rotor-2. The pressure ratio, isentropic efficiency, and mass flow rate of design point are improved 0.93%, 0.57%, and 1.80%, respectively. Also, the results of comparing the performance maps of Optimized Rotor-2 in the choking zone show that at the same pressure ratio equal to 1.3, the mass flow rate of the

Table 5 Performance parameters and its improvement for the optimized rotors.

	Performance Parameters		
	Pressure Ratio	**Isentropic Efficiency**	**Mass Flow Rate [kg/s]**
NASA Rotor-67	1.635	0.922	33.91
Optimized Rotor-1	1.641	0.921	34.17
Optimized Rotor-2	1.650	0.928	34.52

	% Improvement		
	Pressure Ratio	**Isentropic Efficiency**	**Mass Flow Rate**
NASA Rotor-67	---	---	---
Optimized Rotor-1	0.38	-0.13	0.77
Optimized Rotor-2	0.93	0.57	1.80

Table 6 Surge Margin and its improvement for the optimized rotors

	Surge Margin [%]	**Improvement [%]**
NASA Rotor-67	10.618	---
Optimized Rotor-1	11.678	9.98
Optimized Rotor-2	11.133	4.850

Rotor-67 is 34.56 [kg/s] while the Optimized Rotor-2 is 34.95 [kg/s]. The percentage improvement of chocked mass flow rate is equal to 1.13%.

The surge margin (Eqn. (7)) can also be presented as another result of the aerodynamics of the optimal geometries, which is presented in Table 6:

$$Surge\ Margin = 1 - \left(\frac{PR_D}{PR_{NS}}\right) \times \left(\frac{\dot{m}_{NS}}{\dot{m}_D}\right) \quad (7)$$

Another optimization result is the distribution of radial profiles from the hub to the shroud. These on-design performance parameters (pressure ratio, temperature ratio, and isentropic efficiency) for the NASA Rotor- 67, Optimized Rotor-1, and Optimized Rotor-2, and the profiles are presented in Figure 12.

According to the presented results, the hub-to-shroud performance distribution of the two optimized rotors at the design point was improved than the base geometry.

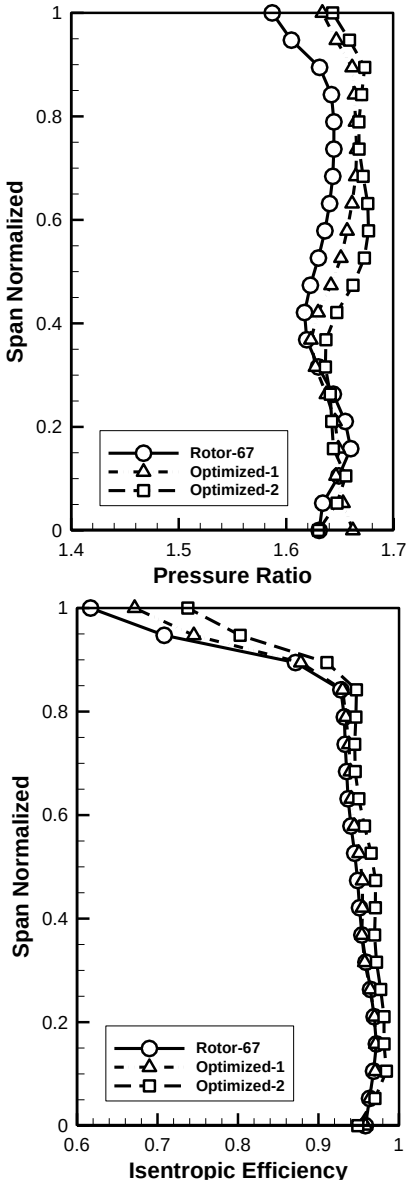

Fig. 13 Comparison of the pressure ratio, and the isentropic efficiency

The maximum improvement of the target parameters occurred near the blade tip.

This improvement in rotor performance can also be achieved by comparing the blade surface pressure distribution at the design point (as shown in Fig. 14). Therefore, the optimal blade loading and the base geometry are extracted in three sections of 10%, 50% and 90% of the blade height and are shown in Fig. 15.

As expected, for the middle section and close to the blade tip ones, the surface pressure loading for the two optimal blades shifted the pressure jump to the trailing edge (in comparison with the base loading), indicating that the shock position was pushed backwards. This has increased the performance of the two optimal geometries.

In addition to the three-dimensional analysis results, the stacking lines, airfoils sections, and the optimized compressors' three-dimensional geometry are compared together. The stacking line for the optimized rotors is presented in Fig. 16.

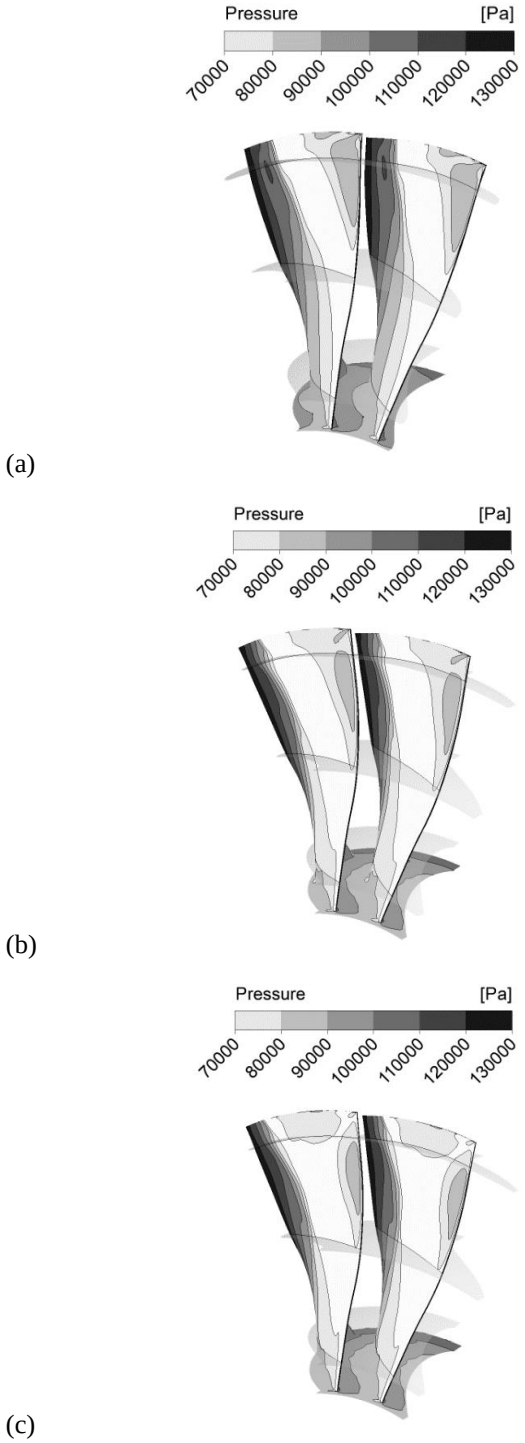

Fig. 14 Comparison of the pressure contour of optimized rotors (b: Optimized Rotor-1), (c: Optimized Rotor-2) with NASA Rotor-67 (a)

The stacking lines of both optimized rotors have a positive sweep with a maximum displacement of 0.529 [cm] and 1.557 [cm] at blade tip for Optimized Rotor-1 and Rotor-2, respectively. The optimized rotors have a positive lean, too. The maximum displacement of Optimized Rotor 1 is seen at the tip of the blade, while the maximum displacement of the Optimized Rotor 2 is at about 70% of the blade span. The comparison of the optimized airfoils with the original Rotor-67 is shown in Fig. 17.

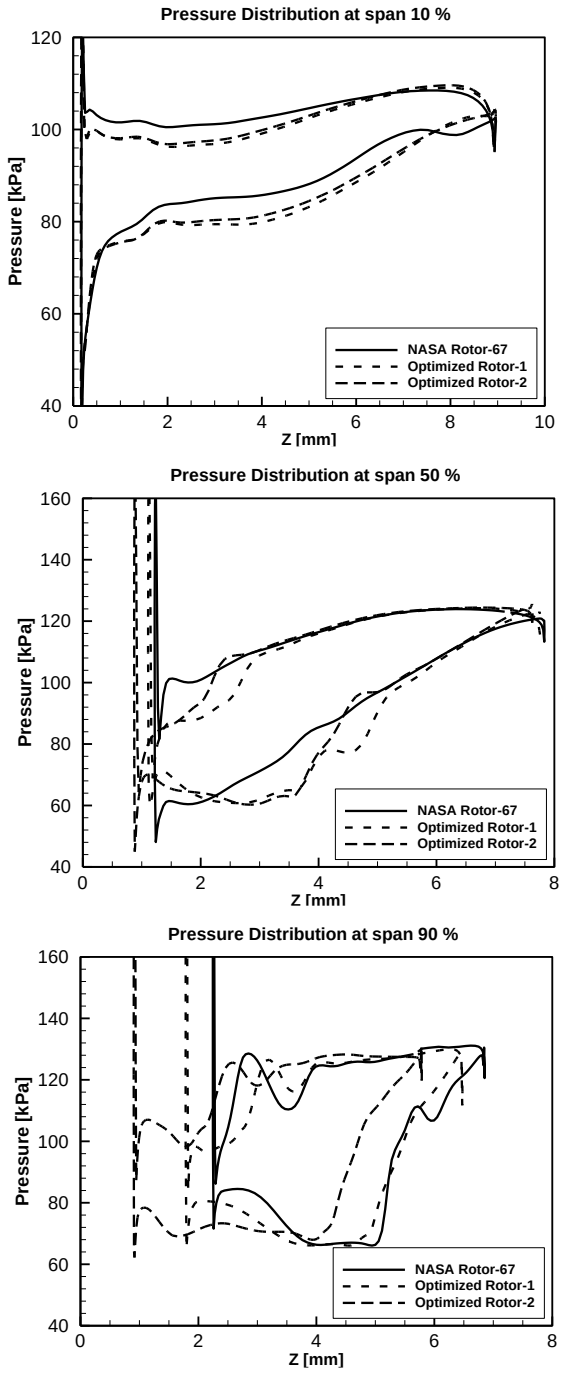

Fig. 15 Comparison of the pressure distribution of optimized rotors with NASA Rotor-67 at span 10%, span 50% and span 90%

According to the presented results, both of the optimized rotors have the same lean and sweep directions. The optimized Rotor-2 has a more positive sweep, while the Optimized Rotor-1 has more curvature in the negative lean direction.

One of the reasons for improving compressor performance using Lean and Sweep is the change in the location of inclined shock on the blade surface. This is because the blade geometry is changed and the inclined shock location is moved toward downstream. Delaying the inclined shock location leads to less losses and improved performance.

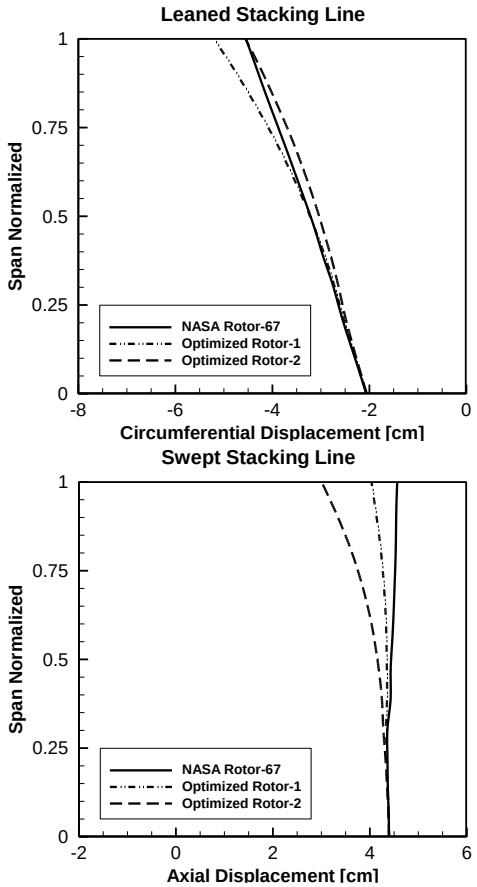

Fig. 16 Comparison of the stacking line for the optimized rotors and NASA Rotor-67

In order to review and compare the performance improvements of axial compressors in numerical optimization processes with the aim of lean and sweep, the results of improving the objective functions have been collected. Table 7 also summarizes the information of previous studies and the results of this research.

Table 7 Summary of lean and sweep optimization results of previous studies and this research

Study	Test Case	Pressure ratio increment [%]	Mass Flow Rate increment [%]	Isentropic Efficiency increment [%]
Benini	Rotor-37	5.5	NA	-0.8
		0	NA	1.5
Oyama	Rotor-67	0.6	0.46	1.78
Samad	Rotor-37	1.62	NA	-0.04
		-1.55	NA	1.41
		1.25	NA	0.51
Wang	Industrial Case	1 %	-0.04	1.1
Huang	Rotor-37	1.4	0.9	0.5
		0.1	0.2	1.2
		0	0.1	1.2
Cao	Rotor-37	0.05	NA	0.8
Present Work	Rotor-67	0.38	0.77	-0.13
		0.93	1.8	0.57

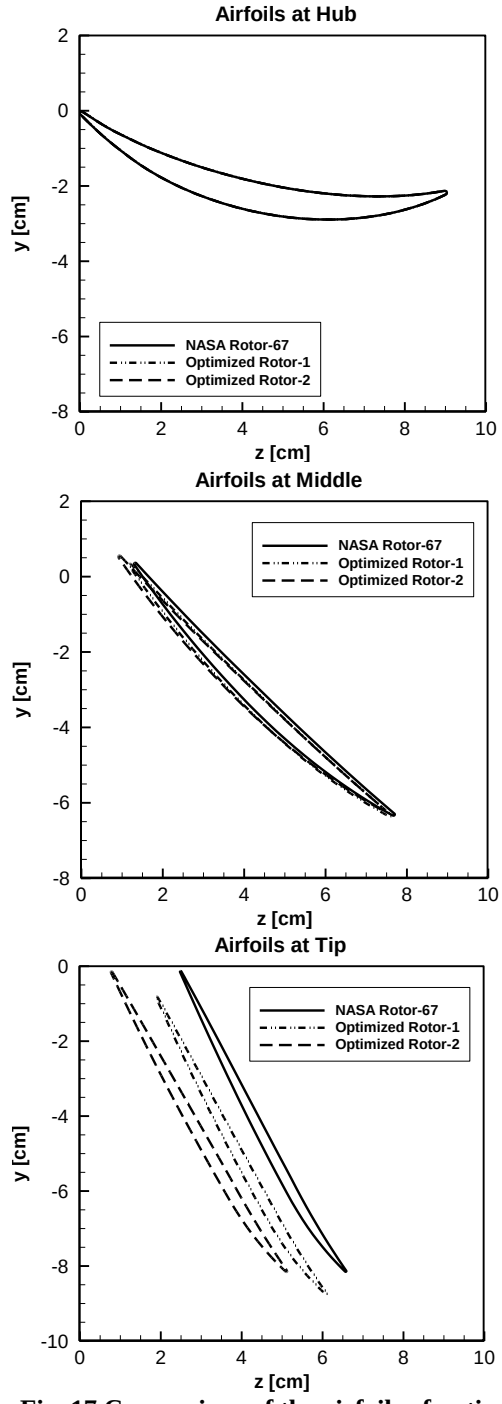

Fig. 17 Comparison of the airfoils of optimized rotors with NASA Rotor-67

It seems that the use of penalties is an important solution to improve the performance of target functions while maintaining other functions (or preventing their reduction).

8. THE ENGINE PERFORMANCE

In the second part of this research, the effect of compressor optimization on a single spool turbojet engine performance is investigated. The thermodynamic cycle analysis of this engine is done at on-design conditions (Cohen et al. 1996), (Saravanamuttoo et al. 2001) and (Friedman et al. 2013). This steady-state analysis of the engine was performed at ground level

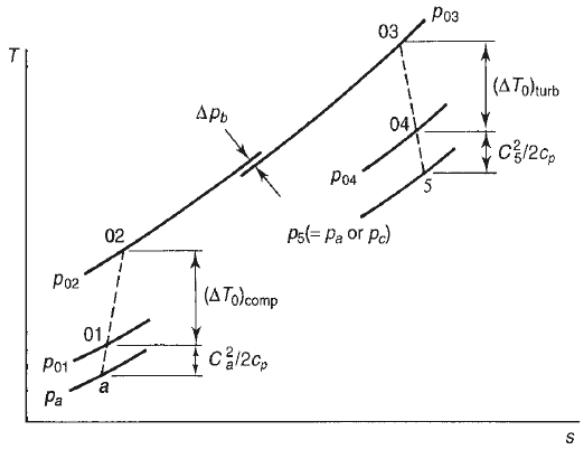

Fig. 18 The actual Turbojet cycle (Cohen et al. 1996; Mattingly, 2006)

conditions (1 [atm] and 288.15 [K]). Figure 18 shows the Brayton thermodynamic cycle of a turbojet engine.

The design specifications of the engine components are summarized in Table 8. The engine's performance characteristics are extracted from an example of GasTurb software (Kruzke, 2018; Kurazke & Halliwell, 2018) whose rotational speed and characteristics are close to the present test case. For the axial compressor, the Rotor-67 is considered the first compressor stage. Therefore, the compressor is divided into two parts, the first stage, and the other multi-stage, with a certain pressure ratio and isentropic efficiency.

To evaluate the effect of optimized geometry on the engine performance, the engine model is simulated in three cases: NASA Rotor-67, Optimized Rotor-1, and

Table 8 The specifications of the turbojet engine

Component		Parameter	Unit	Value
Intake		Total Pressure Ratio	%	99
Compressor	First stage (Rotor-67)	Total Pressure Ratio	---	1.635
		Isentropic Efficiency	%	92.26
	Other stages	Total Pressure Ratio	---	7.34
		Isentropic Efficiency	%	85
Combustor		Burner Efficiency	%	99.5
		Burner Exit Temperature	[K]	1450
		Burner Pressure Ratio	%	97
		Fuel Heat Value	[MJ/kg]	43.124
Turbine		Isentropic Efficiency	%	89
Nozzle		Isentropic Efficiency	%	89

Table 9 Turbojet performance parameters for Rotor-67 and Optimized rotors

	Turbojet Performance		% Improved	
	SFC [g/kN s]	Thrust [kN]	SFC	Thrust
Engine with Rotor-67	26.286	30.16	-	-
Engine With Optimized Rotor 1	26.265	30.38	0.08	0.73
Engine With Optimized Rotor 2	26.231	30.72	0.21	1.86

Rotor-2 are selected as the first stage of the compressor. In these cases, all other engine components' specifications are considered constant and equivalent to the assumed values. Compressor performance improvements for the optimized cases are applied to the engine model, and the cycle is analyzed using the new first-stage compressor. The results are summarized in Table 9.

As shown in Table 9, the Optimized Rotor-2 gives the most improvement in the engine thrust. The engine thrust with the second optimal rotor has increased by 1.86%. Also, the thermodynamic cycle analysis has shown that the specific fuel consumption in both engines (with optimized rotors) has been improved by 0.73 % and 1.86 %, compared to the engine with Rotor-67.

9. CONCLUSION

Optimization of a compressor blade stacking line (lean and sweep) has been accomplished using a Genetic Algorithm coupled with artificial neural networks and a CFD solver. The compressor flow field has been solved by a three-dimensional Reynolds-average Navier-Stokes analysis code (RANS). The result shows the aerodynamic improvement of the objective function for pressure ratio, isentropic efficiency, and mass flow rate at design point is equal to 0.93%, 0.57%, and 1.8%, respectively. The effect of compressor optimization has been investigated on turbojet engine performance using a thermodynamic cycle analysis code. For the best case (Optimized Rotor-2), the engine thrust and SFC are improved by 1.86 % and 0.21 %, respectively.

CONFLICT OF INTEREST

The authors declare no conflict of interest.

AUTHORS CONTRIBUTION

Mojtaba Heidarian Shahri: Software, methodology, validation, formal analysis, data curation, investigation, visualization, writing—original draft preparation. Ali Madadi: Project Administration, supervision, conceptualization, resources, data curation, writing—review and editing. Masoud Boroomand: Project Administration, supervision, conceptualization, resources, data curation, writing—review and editing.

REFERENCES

Benini, E. (2004). Three-dimensional multi-objective design optimization of a transonic compressor rotor. *Propulsion and Power*, 20(3). https://doi.org/10.2514/1.2703

Benini, E., & Biollo, R. (2006). *On the aerodynamics of swept and leaned transonic compressor rotors.* ASME Turbo Expo, Barcelona, Spain. https://doi.org/10.1115/GT2006-90547

Cao, Z., Zhang, X., Liang, Y., & Liu, B. (2021). Influence of blade lean on performance and shock wave/tip leakage flow interaction in a transonic compressor rotor. *Journal of Applied Fluid Mechanics*, *15*(1), 153-167. https://doi.org/10.47176/JAFM.15.01.32753

Cohen, H., Rogers, G., & Saravanamuttoo, H. (1996). *Gas turbine theory* (fourth ed.). London: Longman Group Limited.

Denton, J., & Xu, L. (2002). *The effects of lean and sweep on transonic fan performance.* ASME Turbo Expo, Amsterdam, The Netherlands. https://doi.org/10.1115/GT2002-30327

Ekradi, K., & Madadi, A. (2020). Performance improvement of a transonic centrifugal compressor impeller with splitter blade by three-dimensional optimization. *Energy*, 201. https://doi.org/10.1016/j.energy.2020.117582

Friedman, J., Milton, J., & Karian, J. (2013). *Gas Turbine Aircraft Engine.* New York: The American Society of Mechanical Engineers.

Goswami, S., & Govardhan, M. (2019). Effect of part sweep on axial flow compressor performance in the presence of circumferential casing grooves. *Indian Academy of Sciences*. https://doi.org/10.1007/s12046-019-1176-z

Hah, C., & Wennerstrom, A. (1990). Three-dimensional flowfields inside a transonic compressor with swept blades. *Gas Turbine and Aeroengine Congress and Exposition*, Brussels, Belgium. https://doi.org/10.1115/90-GT-359

Huang, N. Z., Zhao, X., & Zhang, Y. H. (2019). Aerodynamic performance improvement of a transonic axial compressor by swept and leaned rotors. *AIAA Propulsion and Energy 2019 Forum*. https://doi.org/10.2514/6.2019-3819

Jang, C. M., Li, P., & Kim, K. Y. (2005). Optimization of Blade Sweep in a Transonic Axial Compressor Rotor. *JSME International Journal*, 48(4). https://doi.org/10.1299/jsmeb.48.793

Kruzke, J. (2018). *GasTurb 13, design and off-design performance of gas turbines.* Aachen, Germany: GasTurb GmbH.

Kurazke, J., & Halliwell, I. (2018). *Propulsion and Power, An Eploration of Gas Turbine Performance Modeling.* Cham, Switzerland: Springer

International Publishing AG, part of Springer Nature 2018.

Lu, B., Teng, J., Zhu, M., & Qiang, X. (2023). Design optimization of a transonic compressor blade with sweep and lean integrated with axial slot casing treatment. *Aerospace Science and Technology*, 136. https://doi.org/10.1299/jsmeb.48.793

Ma, S. B., Afzal, A., & Kim, K. Y. (2017). Optimization of ring cavity in a centrifugal compressor based on compressor based on comparative analysis of optimization algorithms. *Applied Thermal Engineering*, 262-272. https://doi.org/10.1016/j.applthermaleng.2018.04.094

Mattingly, J. (2006). *Elements of propulsion: Gas turbines and rockets*. Blacksburg, Virginia: American Institute of Aeronautics and Astronautics Inc.

Menter, F., Kuntz, M., & R. Langtry. (2003). Ten years of industrial experience with the SST turbulence model. *The 4th International Symposium on Turbulence, Heat and Mass Transfer*, 10(3), 625-632.

Oyama, A., Liou, M. S., & Obayashi, S. (2004). Transonic axial-flow blade optimization: Evolutionary algorithms/three-dimensional navier–stokes solver. *Propulsion and Power*, 20(4). https://doi.org/10.2514/1.2290

Razavi, S., & Boroomand, M. (2014). Numerical and performance analysis of one row transonic rotor with sweep and lean angle. *Journal of Thermal Science*, 23(5). https://doi.org/10.1007/s11630-014-0727-1

Razavi, S., Sammak, S., & Boroomand, M. (2017). Multi-disciplinary design and optimization of swept and leaned transonic rotor. *Journal of Engineering for Gas Turbines and Power*, 139(12). https://doi.org/10.1115/1.4037456

Samad, A., & Kim, K. Y. (2008). Multi-objective optimization of an axial compressor blade. *Mechanical Science and Technology*, 22. https://doi.org/10.1007/s12206-008-0122-5

Saravanamuttoo, H., Rogers, G., & Cohen, H. (2001). *Gas turbine theory* (fifth ed.). Carleton: Pearson Education.

Strazisar, A., Wood, J., Hathaway, M., & Suder, K. (1989). *Laser anemometer measurements in a transonic axial-flow fan rotor*. Cleveland, Ohio: NASA Lewis Research Center.

Sun, S., Wang, S., Chen, S., Tao, C., Cai, L., & Chen, J. (2019). The impact of various forward sweep angles on the performance of an ultrahigh-load low-reaction transonic compressor rotor. *Applied Thermal Engineering*, 953-966. https://doi.org/10.1016/j.applthermaleng.2019.01.045

Wang, J., He, X., Wang, B., & Zheng, X. (2022). Shapley additive explanations of multi-geometrical variable coupling effect in transonic compressor. *Journal of Engineering for Gas turbines and Power*, 12. https://doi.org/10.1115/1.4053322

Wang, X., Hirsch, C., Kang, S., & Lacor, C. (2011). Multi-Objective optimization of turbomachinery using improved NSGA-II and approximation model. *Computer Methods in Applied Mechanics and Engineering*, 200(9-12), 883-895. https://doi.org/10.1016/j.cma.2010.11.014

Wang, Z., Qu, F., Wang, Y., Luan, Y., & Wang, M. (2020). Research on the lean and swept optimization of a single stage axial compressor. *Engineering Applications of Computational Fluid Mechanics*, 15(1), 142-163. https://doi.org/10.1080/19942060.2020.1862708

Yu, M., Shi, L., Yu, P., & Yao, K. (2022). Robust design of a fan rotor blade by sweep and lean optimization with surface roughness. *Proceedings of the Institution of Mechanical Engineers, Part G: Journal of Aerospace Engineering* https://doi.org/10.1177/09544100221113118